Chapter 9

Fluidic Optical Devices Based on Thermal Lens Effect

Duc Doan Hong
and Fushinobu Kazuyoshi

Additional information is available at the end of the chapter

http://dx.doi.org/10.5772/48072

1. Introduction

Gordon et al. [1] reported that the beam shape of incident laser light expands after passing through a liquid medium. This phenomenon was termed "the thermal lens effect," and it has become a well-known photo-thermal phenomenon. Phenomenological, optical, and spectroscopic studies of the thermal lens effect have been carried out to describe nonlinear defocusing effect [2-8]. Recent progress in laser technology has revealed the various aspects of the thermal lens effect. Based on these efforts, other mechanisms, such as liquid density, electronic population, and molecular orientation, have been found to play important role as well as thermal lens effect. Recent studies term these effects as "the transient lens effect" [9,10]. The main advantage of using the transient lens effect in Photo-Thermal-Spectroscopy is that the sensitivity is 100 to 1000 greater than a traditional absorptiometry [11].

In this research, a new idea of applying the thermal lens effect in order to develop fluidic optical device is proposed. A schematic of the concept is shown in Fig. 1. A rectangular solid region shown in Fig. 1a represents the liquid medium, which has a temperature field generated by a heater-heat sink system or laser-induced absorption. By controlling the temperature field as well as the refractive index distribution of the liquid medium, the refractive angle of each light ray passing through the liquid medium can be controlled in order to develop fluidic optical devices such as: an optical switching in Fig. 1a to change the direction of the input laser beam, a laser beam shaper in Fig. 1b to transform a Gaussian beam to a flat-top beam and a fluidic divergent lens in Fig. 1c. Merits of these devices include flexibility of optical parameters, versatility and low cost.

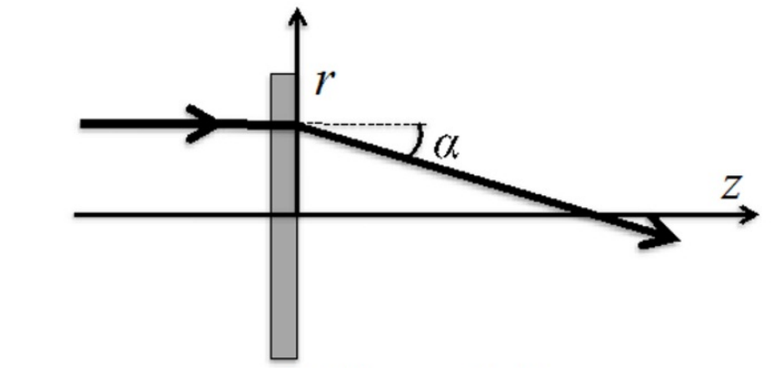

(a) Light ray refraction

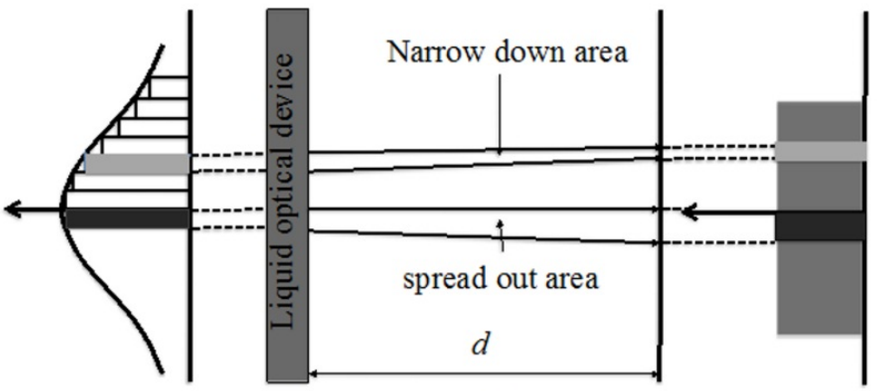

(b) Laser beam shaper

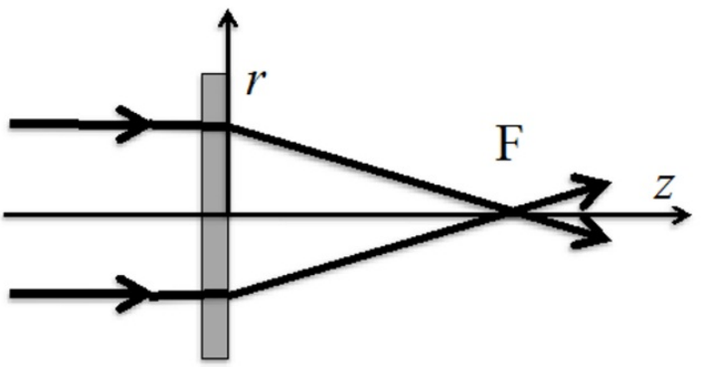

(c) Fluidic divergent lens

Figure 1. Schematic of the concept of the fluidic optical devices

2. Fundamental light ray transmitted in one-dimensional refractive index medium

In this section, as a first step to develop fluidic optical device, the refractive characteristics of a probe beam, which is transmitted in one-dimensional temperature distribution in a liquid medium is presented.

2.1. Theoretical background

The light ray is modeled in the domain shown in Fig. 2 in order to calculate the refractive angle of the probe beam, which is transmitted in a one-dimensional temperature distribution in the liquid medium. The light ray direction transmitted in a medium having a refractive index dependent only on the y-axis, is described by the following form [12]

$$x = \int_0^y \frac{n_0 \sin\theta \cos\varphi}{\sqrt{n^2(y) - n_0^2 \sin^2\theta}} dy \tag{1}$$

$$z = \int_0^y \frac{n_0 \sin\theta \sin\varphi}{\sqrt{n^2(y) - n_0^2 \sin^2\theta}} dy \tag{2}$$

In which, the light ray passes through the medium at coordinate center, θ and ϕ are the incident angle with y and x-axis respectively, n_0 is the refractive index of the medium at the coordinate center.

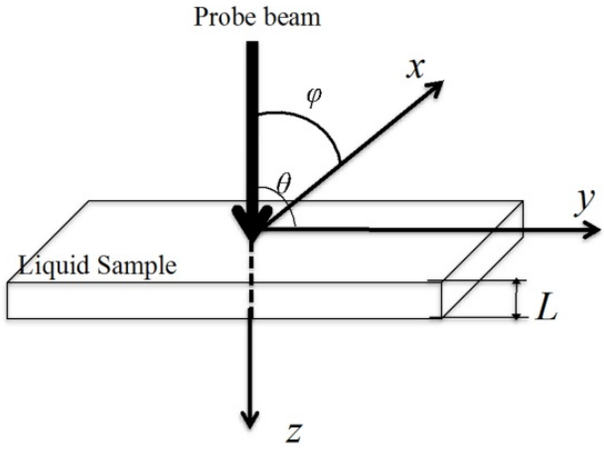

Figure 2. Schematic diagram of computational domain

Figure 2 shows a schematic diagram of the model set up. The rectangular solid medium in the figure represents the domain considered in the calculation which consists of ethylene glycol. In the medium, ethylene glycol has linear temperature distribution in only y-axis direction and the probe beam propagate along z-axis direction. Therefore, $\theta = \phi = \pi/2$, and Eq. (1), (2) become:

$$x = 0 \tag{3}$$

$$z = \int_0^y \frac{n_0}{\sqrt{n^2(y) - n_0^2}} dy \tag{4}$$

The temperature distribution of the liquid medium is modeled with a linear function of the variable y and temperature T at point y is calculated following:

$$T(y) = T_0 + \frac{dT}{dy} y \tag{5}$$

In which, T_0 is the temperature of the liquid medium at coordinate origin and dT/dy is constant.

Furthermore, between 0°C and 100°C refractive index of ethylene glycol is a linear function of temperature with refractive index change dn/dT = -2.6×10^{-4} 1/K [13]. Therefore, the relationship between refractive index and the variable y can be rewriten as follows:

$$y = \frac{n(y) - n_0}{dn / dy} \tag{6}$$

And

$$dy = dn \times \frac{dy}{dn} = dn \times \frac{dy}{dT} \times \frac{dT}{dn} = \frac{dn}{k} \tag{7}$$

Where,

$$k = -2.6 \times 10^{-4} \times \frac{dT}{dy} \tag{8}$$

By substituting Eq. (7) into Eq. (4) and solving the differential equation, we can obtain the relationship between y and z as:

$$y = \frac{n_0[\exp(kz / n_0) - 1]^2}{2k \exp(kz / n_0)} \tag{9}$$

And refractive angle (RA) can be obtained as:

$$\alpha = \frac{dy}{dz} = \frac{1}{2}\exp(\frac{kz}{n_0}) - \frac{1}{2}\exp(-\frac{kz}{n_0}) \tag{10}$$

Equation (10) shows the expression of the refractive angle as a function of the temperature gradient and the thickness of the liquid medium (optical path length). Figure 3 shows the relationship between refractive angle and temperature gradient at points where the thickness of sample, L, is 1.5, 3.0 and 4.5 mm respectively. As shown in Fig. 3 the relationship between the refractive angle and temperature gradient can be well approximated as linear at a small temperature gradient.

2.2. Experimental set-up

Figure 4 shows the experimental set-up to measure the refractive angle. Fluidic optical device in Fig. 4 is a pyrex vessel (internal size: 21×10×L [mm], thickness of the liquid medium, L, can be varied) filled with ethylene glycol. The vessel is held in an adiabatic material (Mica glass-ceramics (Photoveel®) as shown in Fig. 5. The temperature on both sides of the vessel was controlled by a heater-heat sink system to create a one-dimensional temperature distribution in the liquid medium.

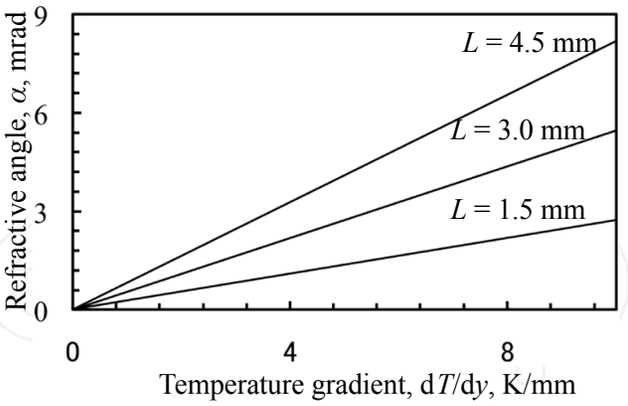

Figure 3. Relationship between the refractive angle and temperature gradient

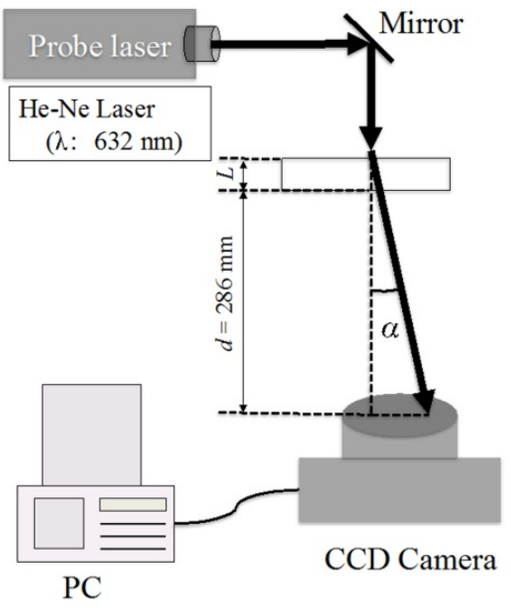

Figure 4. Refractive angle measurement system

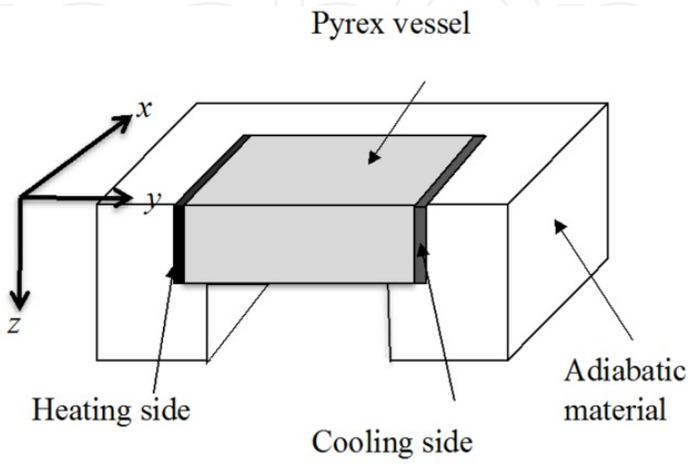

Figure 5. Schematic diagram of sample

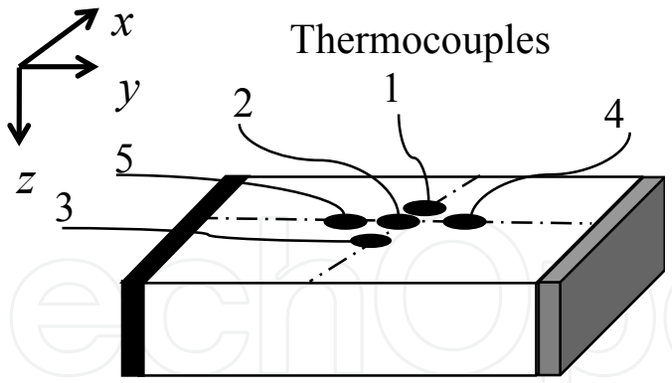

Figure 6. Temperature gradient measurement system

The temperature distribution in the liquid medium is confirmed by measuring the temperatures at 5 points with 2 mm pitch in the vessel using 5 thermocouples as shown in Fig. 6. The temperature gradient in the experiment is given as:

$$\frac{dT}{dy} = \frac{T_4 - T_5}{\Delta y} \tag{11}$$

In which, Δy is the distance between two thermocouples to obtain the temperature gradient, $\Delta y = 4$ mm.

A CW laser ($P = 0.6$ mW, $\lambda = 632$ nm, $\Phi = 0.8$ mm, TEM00) is used as a probe beam. A CCD camera (OPHIR, BeamStar-FX 50) is used as a detector. Based on probe beam position, the refractive angle is estimated with:

$$\alpha = \frac{r}{d} \tag{12}$$

Where d is the distance from the sample to the detector of the camera = 286 mm; r is the beam position.

2.3. Results and discussions

Figure 7(a) and (b) show the comparison of theoretical and experimental results at points where the thickness of sample, L, is 1.5 and 3.0 mm respectively. The temperature gradient in the theoretical results is based on the measurement as described above. As shown in this figure, theoretical and experimental results agree well with each other. The experimental data includes the error corresponding to the difference between the actual temperature gradient at the laser incidence which is calculated by using Eq. (11). The discrepancy at higher dT/dy may correspond to the error where the measured temperature gives higher dT/dy and therefore higher a prediction by using Eq. (10). This discrepancy should increase with increasing sample thickness and the temperature gradient as a consequence of the effect of natural convection and the temperature gradient in the z-axis [14].

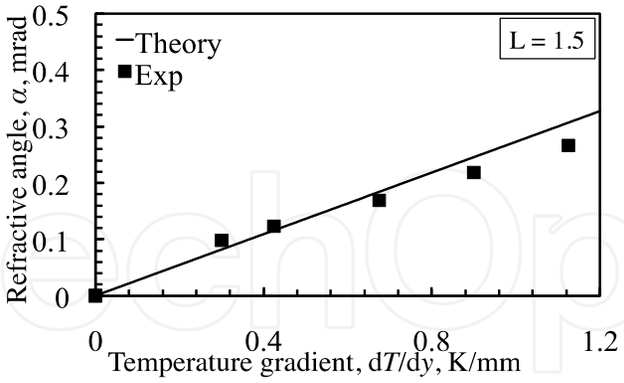

(a) L = 1.5 mm

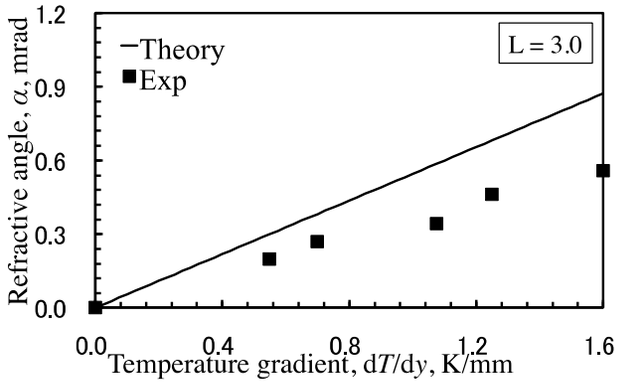

(b) L = 3 mm

Figure 7. The comparison of theoretical and experimental results

3. Fluidic laser beam shaper

Flat-top laser are well known to present significant advantages for laser technology, such as holographic recording system, Z-scan measurement, laser heat treatment and surface annealing in microelectronics and various nonlinear optical processes [15-19]. For CW beams, several approaches to spatially shape Gaussian beams have been developed, such as the use of aspheric lenses, implement beam shaping or the use of diffractive optical devices [20]. However, these methods have some disadvantages: a refractive beam shaping system lead to large aberration [21] and implemental beam shaping has low energy efficiency and lacks of flexibility [22]; and the use of refractive optical devices requires complex configuration design and high cost [23]. In practice, a low-cost and flexible method to convert a Gaussian beam into a flat-top beam is required. In this section, a novel method to convert a Gaussian beam into a flat-top beam is discussed. The concept is based on the control of the pump power and propagation distance of the probe beam in the thermal lens system.

3.1. Principle of thermal lens effect

The principle of the transient lens effect is schematically illustrated in Fig.8. A CW diode pumped blue laser is used as pump-beam (BCL-473-030, λ = 473 nm, Φ = 0.8 mm, TEM_{00}) with maximum output power of 30mW. The laser beam intensity was adjusted by using ND-filter. A CW infrared DPSS laser is used as probe-beam (MIL, λ = 1064 nm, Φ = 3.0 mm, TEM_{00}) with maximum output power of 10 mW. A CCD camera is used as a detector to measure the intensity distribution of the laser beam. A cuvette, which is a three-layer structure with a sheet copper is sandwiched between 2 pieces of fused silica. The height of the fused silica is 1 mm. The sheet copper has doughnut shape. The liquid that is contained inside the doughnut hole has the same height with the sheet copper. By varying the thickness of the sheet copper, the liquid height can be changed. The ethanol solution dissolved dye termed as Sunset-yellow is filled in the cuvette. The chemical formula of the Sunset-yellow is shown in Ref. 24.

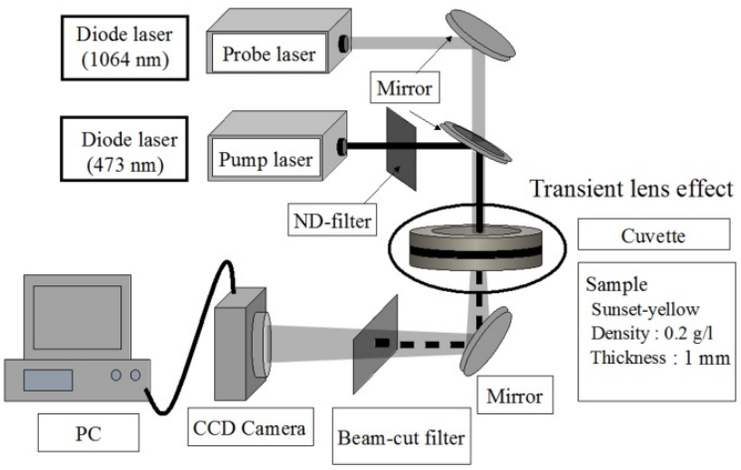

Figure 8. Schematic diagram of a dual-beam thermal lens system

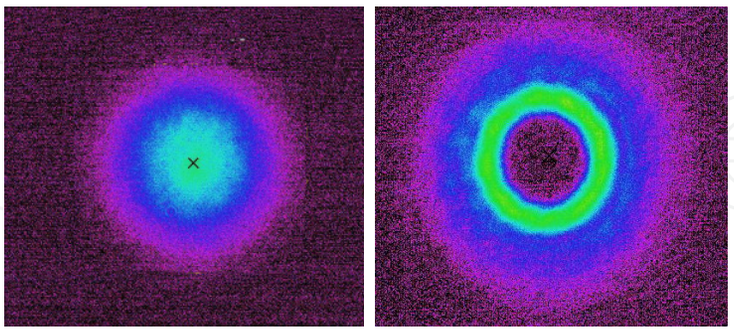

Figure 9. Experiment result: the difference of intensity profile of the probe beam after passing through the thermal lens (left side) and a quart divergent lens (right side)

In this experiment, the absorbance of the pump-beam is 2.776 and that of the probe-beam is negligible small. Figure 9 shows the laser beam profile of the probe beam after propagating through a divergent lens and a thermal lens. It is clear that, the probe beam change its profile from Gaussian to doughnut beam with a hollow center is created.

Theoretical analysis of laser beam profile change in thermal lens effect is done with a model that includes continuity equation, Navier-Stokes equation, energy conservation equation and Helmholtz equation in 2D cylindrical symmetry coordinate. It is assumed that the change of refractive index is caused only by the temperature change of the liquid medium and the thermal coefficient of the refractive index, dn/dT. The concentration is supposed to be constant over the range of the temperature rise induced by the pump beam. When the liquid medium is irradiated, temperature distribution perpendicular to the optical axis is formed due to intensity distribution of laser beam and heat transport. To consider the natural convection effect, the temperature distribution of liquid sample in steady state is calculated numerically following these governing equations [24]:

$$\frac{1}{r}\frac{\partial}{\partial r}\left(rv_r\right)+v_z\frac{\partial v_z}{\partial z}=0 \tag{13}$$

$$\begin{aligned} v_r\frac{\partial v_r}{\partial r}+v_z\frac{\partial v_r}{\partial z}&=-\frac{1}{\rho}\frac{\partial p}{\partial r}+\nu\left(\frac{\partial}{\partial r}\left(\frac{1}{r}\frac{\partial}{\partial r}\left(rv_r\right)\right)+\frac{\partial^2 v_r}{\partial z^2}\right) \quad (a)\\ v_r\frac{\partial v_z}{\partial r}+v_z\frac{\partial v_z}{\partial z}&=-\frac{1}{\rho}\frac{\partial p}{\partial z}+\nu\left(\frac{1}{r}\frac{\partial}{\partial r}\left(r\frac{\partial v_z}{\partial r}\right)+\frac{\partial^2 v_z}{\partial z^2}\right)+g\beta\left(T-T_0\right) \quad (b)\end{aligned} \tag{14}$$

$$v_r\frac{\partial T}{\partial r}+v_z\frac{\partial T}{\partial z}=a\left(\frac{1}{r}\frac{\partial}{\partial r}\left(r\frac{\partial T}{\partial r}\right)+\frac{\partial^2 T}{\partial z^2}\right)+S \tag{15}$$

$$S=\frac{\alpha \mathrm{e}^{-\alpha z}I_0(r)}{\rho \mathrm{C}_\mathrm{p}} \tag{16}$$

Here, $I_0(r)$ is the intensity distribution of the pump laser. The spot sizes of the laser beams are assumed to be constant through the interaction volume within the liquid medium.

The temperature distribution is calculated numerically based on the finite difference method. The 1st order upwind scheme and a 2nd order center differencing are applied to discretize the advection term and the diffusion term respectively. The thermal properties of liquid medium can be found in Ref. 24.

To model the propagation of laser through an inhomogeneous medium, the wave equation which includes an absorption term and an inhomogeneous refractive index term is applied [24]:

$$-\frac{\partial^2 E}{\partial z^2}+2ik_0n_0\frac{\partial E}{\partial z}=\frac{1}{r}\frac{\partial}{\partial r}\left(\frac{\partial(rE)}{\partial r}\right)+k_0^2\left(n^2-n_0^2\right)E-\frac{1}{2}ik_0n_0\alpha E \tag{17}$$

Here, E is the envelope of the oscillating electric field, z is the axis of propagation, r is transverse coordinates, k_0 is the free space wave number and α is the absorption coefficient. The variable n is the refractive index profile depending on medium temperature following:

$$n(T) = n_0 + \frac{dn}{dT}\left(T - T_0\right) \tag{18}$$

Here, n_0 = 1.359 is the refractive index of the liquid medium at reference temperature T_0 = 298.15 K, dn/dT is the temperature coefficient of the refractive index. The propagation of laser is calculated based on Pade method. The optical properties parameter can be found in Ref. 24.

3.2. Influences of the pump power and the propagation distance on the change of probe beam profile

Influences of the pump power and the propagation distance to the probe beam profile were investigated numerically using the calculation parameters in Table. 1. In this calculation, both of the pump beam and the probe beam are written as follows.

$$E = E_0 \exp\left(\frac{-r^2}{r_0^2}\right)\exp\left(\frac{-ik_0 n_0 r^2}{2R}\right) \tag{19}$$

$$E_0 = \sqrt{\frac{2P}{\pi r_0^2}} \tag{20}$$

Here P is the power of laser, R is the radius of curvature of the wave front, r and r_0 are distance from laser axis and beam radius respectively.

Parameter	(a)	(b)
Pump power, mW	3	0 ~ 7
Pump beam diameter, mm	0.8	0.8
Probe power, mW	10	10
Probe beam diameter, mm	0.8	0.8
Absorption coefficient, cm^{-1}	2.0	2.0
Distance from experimental section to CCD camera, mm	0 ~ 500	200
Phase front curvature radius, R, mm	∞	∞

Table 1. Calculation conditions

Effects of the pump power and the propagation distance to the probe beam profile are shown in Fig. 10(a) and (b) respectively. The vertical axis and horizontal axis show intensity and distance from laser axis respectively. Plots of 'P = 0 mW' and 'd = 0 mm' represent intensity distribution of the probe beam without thermal lens effect. As shown in Fig. 10(a), the further the propagation distance, the lower intensity at the probe beam center, and higher intensity at the wing. With increasing of the propagation distance, the laser beam profile changes from Gaussian to flat-top and the doughnut beam profile respectively. The profile of the probe beam changes with the same tendency as the increasing of pump power as shown in Fig. 10(b). In particular, when the pump power is 3 mW and propagation

distance is 200 mm the probe beam is converted to the flat-top profile approximately. Therefore, by controlling the pump power and the propagation distance the Gaussian beam can be converted into the flat-top beam.

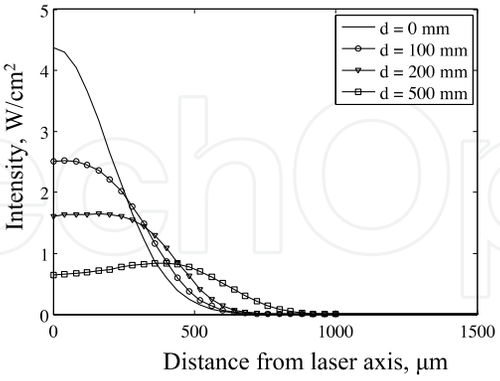

(a) Influence of the propagation distance

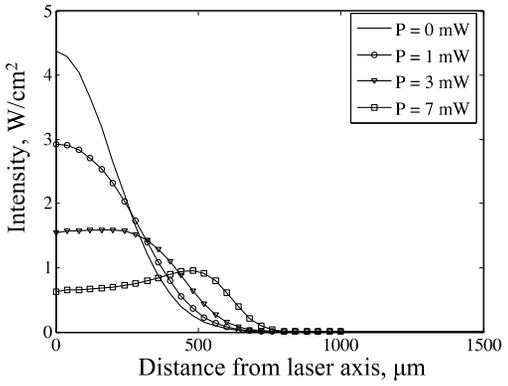

(b) Influence of the pump power

Figure 10. Influence of the propagation distance and the pump power to the probe beam profile

3.3. Experimental set-up to shape spatial profile

In order to confirm the role of the fluidic laser beam shaper, a single-beam experiment is set up as shown in Fig. 11. A CW diode blue laser is used as pump and probe-beam (P = 10 mW, λ = 488 nm, Φ = 0.69 mm, TEM00). In this experiment, the height of the liquid medium is 0.5 mm, the dye concentration is 0.1 g/l and the absorption coefficient is 2.92 cm^{-1} (measured value) respectively. The propagation distance to obtain the flat-top beam profile is measured by changing the distance from the cuvette to the CCD camera. At the propagation distance of 150 mm, the flat-top beam is confirmed as shown in Fig. 12(a).

Figure 12(b) shows the beam profile change from the Gaussian to the flat-top beam. The vertical and horizontal axes show the intensity and distance from the laser axis respectively. The o-line shows the profile of the Gaussian input beam by fitting the laser beam profile measured at the surface of the cuvette. The strange-line shows the profile of the flat-top beam calculated by beam propagation method. The solid-line shows the profile of the flat-

top beam measured by CCD camera at propagation distance of 150 mm from the cuvette. Both experimental and calculated results agree well with each other.

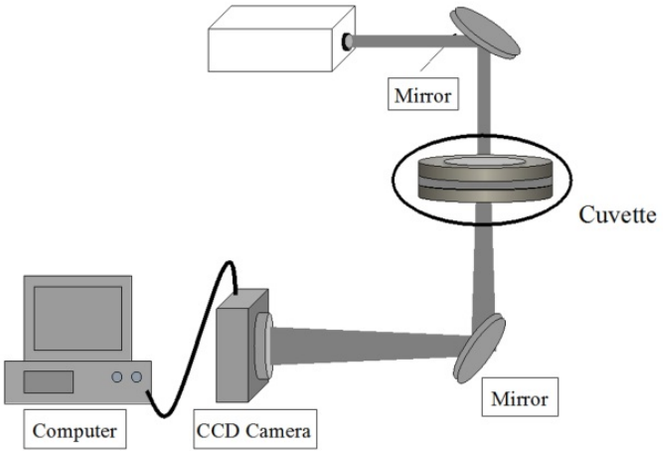

Figure 11. Experimental set up for a single-beam thermal lens system to transfer a Gaussian beam to flat-top beam

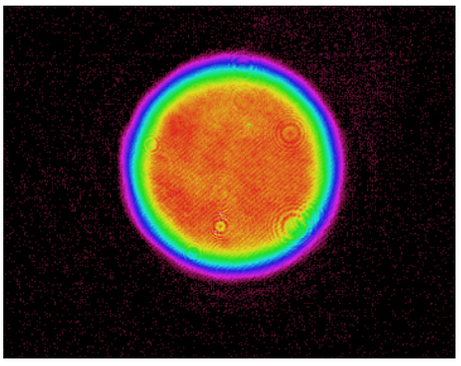

(a) Flat-top beam profile measured by CCD camera

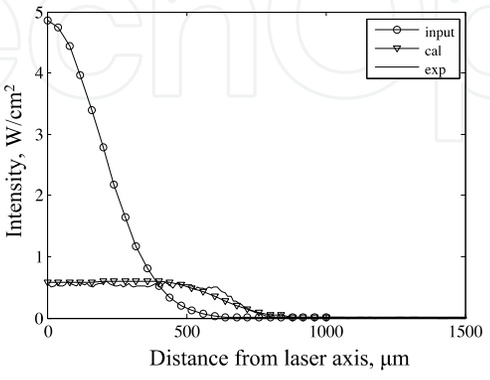

(b) Beam profile change from Gaussian to flat-top

Figure 12. Experimental results

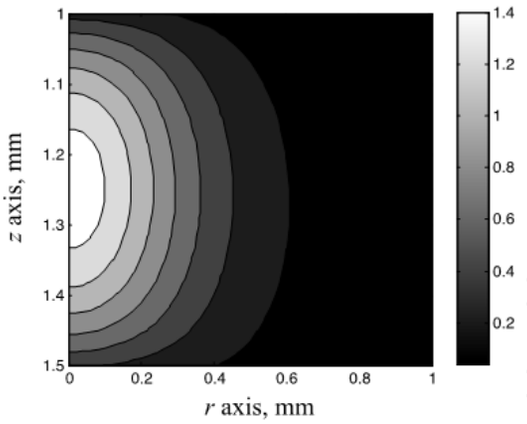

Figure 13. Temperature distribution inside the liquid medium [K]. The calibration shows the difference between temperature inside the liquid medium with the ambient temperature.

In order to explain in more detail about the mechanism of this fluidic beam shaper, the temperature distribution of liquid medium is calculated. As shown in Fig. 13, local heating near the beam axis produces a radially dependent temperature variation, which changes the liquid refractive index in which the lower refractive index is in the region near to the beam center. As a consequence, the radius of curvature of the wave front at the region near the beam center is shorter than one at the beam wing. Therefore the sample liquid locally acts as a micro divergent lens with shorter focal length at beam center. As shown in Fig. 1b, the beam center that passes through shorter focal length is spread out more rapidly than the beam wing. As the probe beam propagates to increasing distance, the intensity in the center region drops rapidly than one in the wing region. At a certain value of propagation distance, the Gaussian beam can be converted into the flat-top beam.

It is noted that, in the case of single-beam shaper, one part of laser beam energy (about 15% in this experiment) is converted into thermal energy in order to change temperature distribution or in other words to change refractive index distribution in the liquid medium. Therefore, in the case of single-beam shaper, the beam shaper has another role, which is as an attenuator. This laser beam shaper/attenuator can be applied in practical laser drilling technology. In the case of applying on only laser beam shaper, the double-beam system is recommended. In this case, it is needed to select dye whose absorbance of the probe-beam is negligible small.

3.4. Relationship between pump power and distance to shape spatial profile

As shown in previous section, the flat-top beam can be obtained only at a fixed distance. In order to control this distance, the influence of pump power is investigated theoretically and experimentally. The calculation parameters are shown in Table. 2. The pump power is changed from 1 to 8 mW. The distance to obtain the flat-top beam is obtained numerically. The relationship between the pump power and the distance to shape spatial profile is shown in Fig. 14(a). The horizontal and vertical axes show pump power and distance to obtain the flat-top beam respectively. As shown in Fig. 14(a), the distance to obtain a flat-top beam is in inverse proportion to the pump power.

In order to validate the numerical prediction, a single beam experiment was carried out. The pump power is changed from 1 to 6 mW and the distance to obtain the flat-top beam was measured. The experimental result shown in Fig. 14(b), shows excellent agreement with calculation prediction. The relationship between pump power and distance to obtain the flat-top beam can be explained by the interaction between energy absorption of liquid medium with the focal length of local micro lens. As the pump power increase, the absorption energy increases. As a consequence, the rate of decreasing of R is enhanced. This can be thought as the reason why the distance to obtain a flat-top beam decreases. In other words, the distance to obtain the flat-top beam profile also decreases with the increasing of absorption coefficient. Therefore, by changing the absorption coefficient or the pump power, the distance to obtain a flat-top beam can be controlled.

Pump power, mW	1 ~ 8
Pump beam diameter, mm	0.8
Probe power, mW	10
Probe beam diameter, mm	0.8
Absorption coefficient, cm^{-1}	2.0
Phase front curvature radius, R, mm	320

Table 2. Calculation conditions

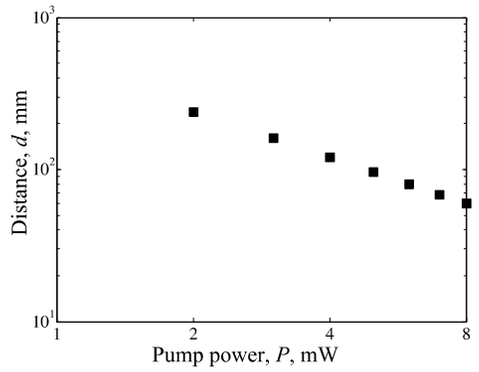

(a) Calculation result

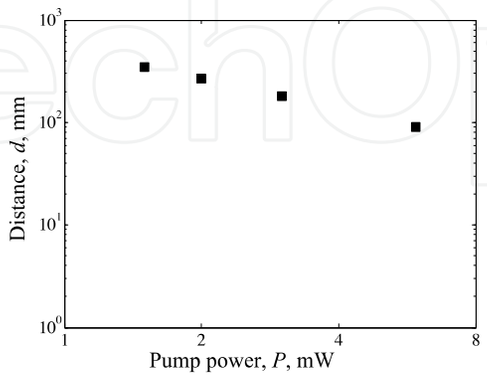

(b) Experimental result

Figure 14. Relationship between the pump power and the distance to obtain the flat-top beam profile. The horizontal and vertical axes show the pump power and the distance to obtain the flat-top beam profile respectively.

4. Tunable fluidic lens

Fluidic lenses are well known to present significant advantages for wide range of applications from mobile phone to laboratory on a chip. Fluidic lenses have a number of apparent advantages such as tunable refractive index and reconfigurable geometry. Several approaches to design the liquid lens have been developed based on the microfluidic techniques to modify the liquid lens shape by using: out-of-plane micro-optofluidic [25-26], in-plane micro-optofluidic [27-28], electron wetting [29], dielectrophoresis [30] and hydrodynamic force [31]. Other approach bases on turning the refractive index of the liquid by different means such as pressure control, optical control, magnetic control, thermo-optic control, and electro-optic control.

4.1. Principle of fluidic lens

When the liquid medium is irradiated, local heating near the beam axis produces a radially dependent temperature variation, which changes the liquid refractive index in which the lower refractive index is in the region near to the beam center. As a consequence, the radius of curvature of the wave front at the region near the beam center is shorter than one at the beam wing. The liquid medium behaviors as a convergence GRIN-L with focal length depends on the radial position of the incident ray relative to the optical axis of the cuvette. The ray equation that is calculated numerically to obtain the path of an incident beam, which is given by:

$$\frac{d}{ds}\left(n\frac{dR}{ds}\right)=\text{grad}(n) \tag{21}$$

Where, ds and R are the differential element of the path length and the positional vector of the ray respectively. The variable n is the refractive index of the liquid sample. The variable n is the refractive index profile depending on medium temperature following equation (13-16, 18).

4.2. Influences of the pump beam profile

Influences of the pump beam profile to the focal length of the GRIN-L were investigated numerically with the calculation conditions in Table. 3. The intensity profile of the pump is applied with the Gaussian beam and the quasi-flat-top beam (a super-Gaussian distribution of order k) using Eq. 22 and Eq. 23 respectively.

$$I_{\text{Gaussian}}=\frac{2P}{\pi r_0^2}\exp\left(\frac{-2r^2}{r_0^2}\right) \tag{22}$$

$$I_{\text{Flat-top}}=\frac{Pk2^{2/k}}{2\pi r_0^2\Gamma(2/k)}\exp\left(\frac{-2r^k}{r_0^k}\right) \tag{23}$$

Here Γ is the Gamma function, r and r_0 are distance from laser axis and beam radius, respectively. In this calculation, quasi-flat-top beam is the 10 order of the super-Gaussian distribution, two types of the pump intensity profile are shown in Fig.15.

Pump power, mW	10
Pump beam diameter, mm	1.5
Absorption coefficient, cm^{-1}	2.0

Table 3. Calculation conditions

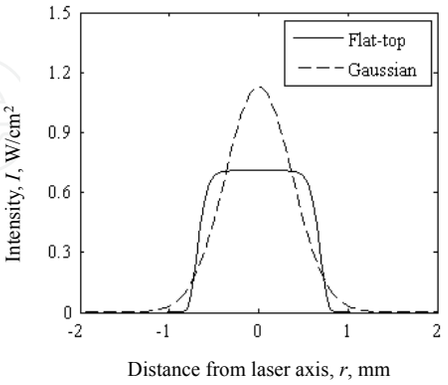

Figure 15. Two types of the pump beam profile

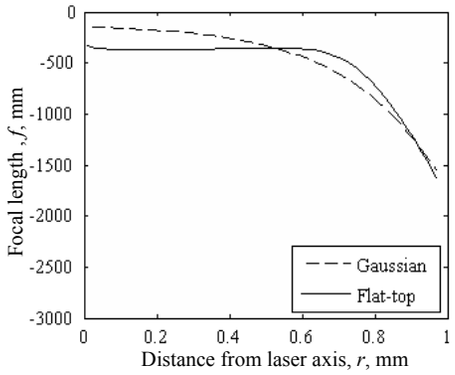

Figure 16. Effect of the pump beam profile to the focal length of the GRIN-L lens

The effect of the pump beam profile to the focal length of the GRIN-L lens is shown in Fig. 16. The vertical and horizontal axes show focal length and distance from laser axis respectively. The solid and dashed lines represent the plot of the focal length again the radial position of the incident ray relative to the optical axis of the cuvette in the case of Gaussian pump beam and quasi flat-top pump beam respectively. As shown in Fig. 16, for the Gaussian pump beam the focal length of the GRIN-L increases sharply with increasing of the distance from laser axis, which means larger spherical aberration. It means that, the beam center which passes through shorter focal length is spread out more rapidly than the beam wing. As a consequence, the further the propagation distance of the probe beam, the laser beam profile changes from Gaussian to the doughnut beam profile [24], which should cause some undesirable results in laser processing [32]. In contrast, with the quasi flat-top pump beam, the focal length of the GRIN-L varies lightly with increasing of the distance from laser axis smaller than beam waist of the flat-top pump beam. The area smaller than the beam waist of the flat-top pump beam acts as a divergent lens with small spherical aberration. Therefore, for the purpose of designing the GRIN-L lens the uniform pump beam shows the advance in reducing the spherical aberration.

4.3. Experimental set-up

In order to confirm the qualities of the GRIN-L, an experiment with the quasi flat-top pump beam is carried out as shown in Fig. 17. A CW diode blue laser is used as pump laser (P = 10 mW, λ= 488 nm, Φ = 0.69 mm, TEM00). In cuvette 1, the height of liquid is 0.5 mm, and the absorption coefficient is 2.92 cm^{-1} (at wavelength of 488 nm). In the cuvette 2, the height of liquid is 1 mm, and the absorption coefficient is 55 cm^{-1} (at wavelength of 488 nm). A CW He-Ne laser is used as probe laser (P = 0.6 mW, λ = 632 nm, Φ = 0.8 mm, TEM00). It is noted that, the absorption of ethanol solution can be ignored at the wavelength of the probe laser. First, the pump beam passes through cuvette1, then the beam profile of pump beam was converted from Gaussian to flat-top during its transmission to cuvette 2 as shown in Fig. 18. Then, the probe laser was adjusted to overlap with pump laser. After propagating through

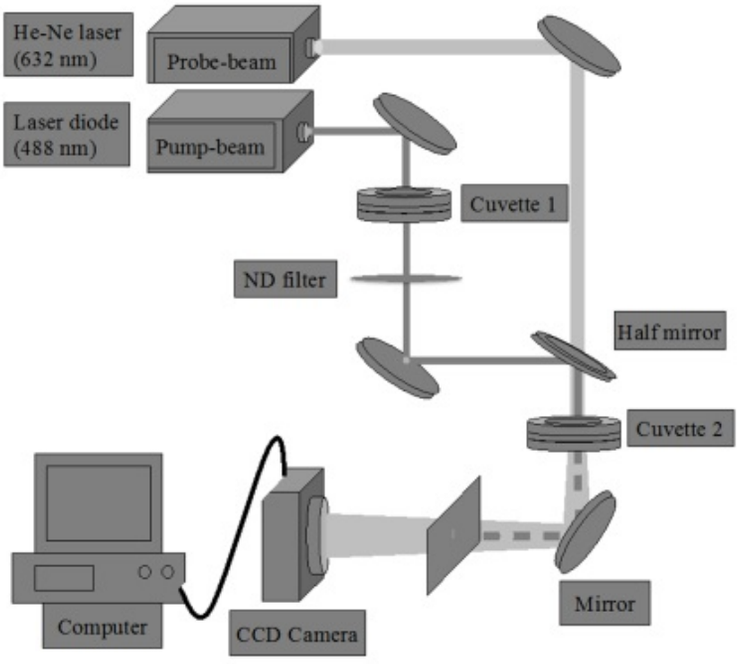

Figure 17. Experimental set-up for the fluidic divergent lens

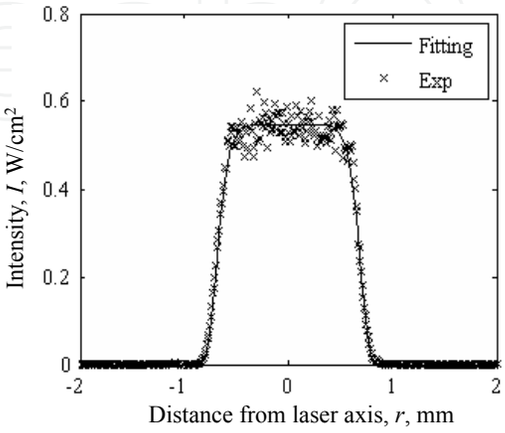

Figure 18. The intensity profile of the pump beam during its transmission to cuvette 2. Dotted and solid lines show the measured result and fitting by super-Gaussian distribution respectively.

the sample the probe laser is directed towards the CCD camera and the pump laser is blocked using filters located at the detection plane. The distance between cuvette 2 and the CCD camera is varied, and the $1/e^2$ diameter of probe laser is measured.

Figure 19(a) shows the change along the propagation direction in the beam profile. The vertical and horizontal axes show the intensity and distance from the laser axis respectively. By using the quasi flat-top pump beam, the beam profile of probe laser can remain in Gaussian distribution during its propagation. Figure 19(b) shows the plot of probe beam waist again propagation distance. As shown in Fig. 19(b), the beam waist of probe laser varies linearly with propagation distance. In other words, cuvette 2 acts as a divergence lens with focal length of f = -424 mm (this value has been calculated by considering the divergence angle of probe laser θ = 1.2 mrad).

Next, the pump power is changed from P_0 = 7.7 mW to $P_0/2$, $P_0/3$ and $P_0/4$ respectively. Figure 20 shows the plots of focal length against the pump power. Square and circle plots show the calculation and experimental result, respectively. As shown in Fig. 20, the focal length increases with increasing of the pump power. This means that, by adjusting the pump power, the focal length can be controlled.

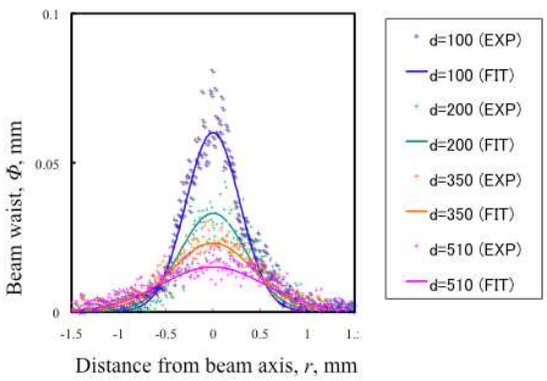

(a) Beam profile

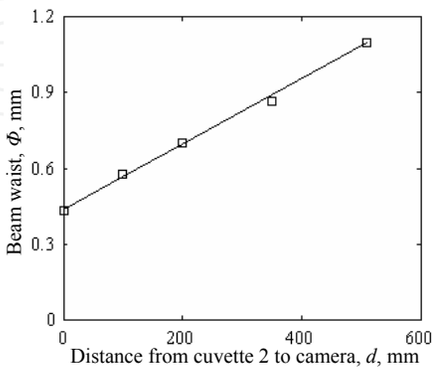

(b) Beam waist

Figure 19. Probe beam changes along the propagation direction

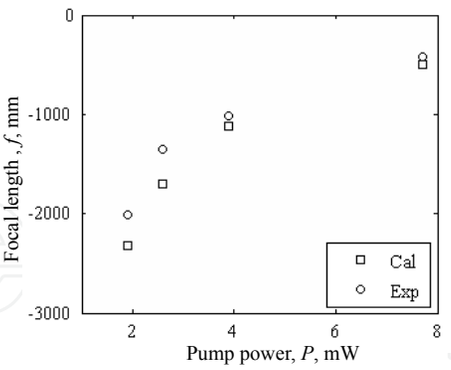

Figure 20. Relationship between the pump power and focal length

5. Conclusion

In this research, a novel idea of fluidic optical devices which includes laser beam shaper and fluidic divergent lens are demonstrated. The fluidic optical devices are based on controlling some parameters in the thermal lens system. The interaction among the intensity distribution, power of the pump beam, the absorption coefficient, the propagation distance and the intensity profile of the probe beam have been investigated experimentally and theoretically. It is found that

- By controlling the pump power and the absorption coefficient, the input Gaussian beam can be converted into a flat-top beam profile. The distance to get the flat-top beam profile can be controlled easily by adjusting the pump power and the absorption coefficient. In actual applications, single-beam shaper has another role, which is as an attenuator. This laser beam shaper/attenuator can be applied in practical laser drilling technology. In the case of applying on only laser beam shaper, the double-beam system is recommended. In this case, it is needed to select a dye whose absorbance of the probe-beam is negligible small.
- The uniform pump beam shows the advance in reducing the spherical aberration. And by adjusting the pump power, the focal length can be controlled

With some merits such as flexiblility, versatility and low cost, these fluidic optical devices will be promising tools in many fields of laser application.

Author details

Hong Duc Doan and Kazuyoshi Fushinobu
Department of Mechanical and Control Engineering,
Tokyo Institute of Technology,
Meguro-ku, Tokyo,
Japan

Acknowledgement

Part of this work has been supported by the Grant-in-Aid for JSPS Fellows and Grant-in-Aid for Scientific Research of MEXT/JSPS. The authors also would like to acknowledge Mr. Akamine Yoshihiko.

6. References

[1] J. P. Gordon, R. C. C. Leite, R. S. Moore, S. P. S. Porto, and J. R. Whinnery, Long-Transient effects in lasers with inserted liquid samples, J. Appl. Phys. 36 (1965) 3-8

[2] S.A. Akhmanov, D.P. Krindach, A.V. Migulin, A.P. Sukhorukov and R.V. Khokhlov, Thermal self-actions of laser beams, IEEE J. Quantum Electronics QE-4 (1968) 568-575

[3] P. M. Livingston, Thermally induced modifications of a high power CW laser beam, Appl. Opt. 10 (1971) 426-436

[4] J. F. Power, Pulsed mode thermal lens effect detection in the near field via thermally induced probe beam spatial phase modulation: a theory, Appl. Opt. 29 (1990) 52-63

[5] P. P. Banerjee, R. M. Misra, and M. Maghraoui, Theoretical and experimental studies of propagation of beams through a finite sample of a cubically nonlinear material, J. Opt. Soc. Am. B 8 (1991) 1072-1080

[6] J. M. Hickmann, A. S. L. Gomes, and C. B. de Araújo, Observation of spatial cross-phase modulation effects in a self-defocusing nonlinear medium, Phys. Rev. Lett. 68 (1992) 3547–3550

[7] Govind P. Agrawal, Transverse modulation instability of copropagating optical beams in nonlinear Kerr media, J. Opt. Soc. Am. B 7 (1990) 1072-1078

[8] C. J. Rosenberg et al., Analysis of the dynamics of high intensity Gaussian laser beams in nonlinear de-focusing Kerr media, Optics Communications 275 (2007) 458–463

[9] M. Sakakura, and M. Terazima, Oscillation of the refractive index at the focal region of a femtosecond laser pulse inside a glass, Opt. lett. 29 (13) (2004) 1548-1550

[10] M. Sakakura, and M. Terazima, Real-time observation of photothermal effect after photo-irradiation of femtosecond laser pulse inside a glass, J. Phys. France 125 (2005) 355-360

[11] M. Terazima, N. Hirota, S. E. Braslavsky, A. Mandelis, S. E. Bialkowski, G. J. Diebold, R. J. D. Miller, D. Fournier, R. A. Palmer, and A. Tam, Quantities, terminology, and symbols in photothermal and related spectroscopies (IUPAC Recommendations 2004), Pure Appl.Chem. , 76, 1083

[12] Kudou Uehara 1990, Basic Optics (Kougaku Kiso) Gendaikougaku, Tokyo, Japan, p. 45-47 (Japanese)

[13] S. K. Y. Tang, B. T. Mayers, D. V. Vezenov, and G. M. Whitesides, Optical waveguiding using thermal gradients across homogeneous liquids in microfluidic channels, *Appl. Phys. Lett.* 88, 06112, 2006

[14] H. D. Doan, K. Fushinobu, and K. Okazaki, Investigation on the interaction among light, material and temperature field in the transient lens effect, transmission characteristics in 1D temperature field, Proc. ITherm 2010, No. 127.
[15] J. Yang, Y. Wang, X. Zhang, C. Li, X. Jin, M. Shui, and Y. Song, Characterization of the transient thermal-lens effect using flat-top beam Z-scan, J. Phys. B: At. Mol. Opt. Phys. 42 (2009) 225404 (5pp)
[16] K. Ebata, K. Fuse, T. Hirai, and K. Kurisu, Advanced laser optics for laser material processing, Proc. SPIE, Vol. 5063, 411 (2003)
[17] E. B. S. Govil, J. P. Longtin, A. Gouldstone and M. D. Frame, Uniform-intensity, visible light source for *in situ* imaging, Journal of Biomedical Optics 14(2) (2009) 024024-024024-7
[18] F. M. Dickey, S. C. Holswade and D. L. Shealy 'Laser Beam Shaping Applications', Taylor & Francis, 2006
[19] M. T. Eismann, A. M. Tai and J. N. Cederquist, Iterative design of a holographic beam former, Appl. Opt. 28 (1998) 2641-1650
[20] F. M. Dickey and S. C. Holswade, Laser beam shaping: Theory and Techniques, Marcel Dekker, New York, 2000
[21] P. Scott, Reflective optics for irradiance redistribution of laser beam design, Appl. Opt. 20 (9) (1981) 1606-1610
[22] S. Zhang, Q. Zhang and G. Lupke, Spatial beam shaping of ultrashort laser pulse: theory and experiment, Appl. Opt.44 (2005) 5818-5823
[23] B. Mercier, J.P. Rousseau, A. Jullien, L. Antonucci, Nonlinear beam shaper for femtosecond laser pulses, from Gaussian to flat-top profile, Optics Communications 283 (2010) 2900-2907
[24] H. D. Doan, Y. Akamine, K. Fushinobu, Fluidic laser beam shaper by using thermal lens effect, Int. J. Heat Mass Transfer (2012) 55 2807–2812
[25] S. H. Ahn, Y. K. Kim, Proposal of human eye's crystalline lens-like variable focusing lens, Sens. Actuators (1999), A 78**,** 48
[26] D. Y. Zhang, V. Lien, Y. Berdichevsky, J. H. Choi, Y. H. Lo, Fluidic adaptive lens with high focal length tenability, Appl. Phys. Lett. 82 (2003), 3171
[27] S. K. Hsiung, C. H. Lee, and G. B. Lee, Microcapillary electrophoresis chips utilizing controllable micro-lens structures and buried optical fibers for on-line optical detection, Electrophoresis (2008) 29, 1866
[28] V. Lien, Y. Berdichevsky, Y. H. Lo, Microspherical surfaces with predefined focal lengths fabricated using microfluidic capillaries, Appl. Phys. Lett. (2003) 83, 5563
[29] C. B. Gorman, H. A. Biebuyck, G. M. Whitesides, Control of the Shape of Liquid Lenses on a Modified Gold Surface Using an Applied Electrical Potential across a Self-Assembled Monolayer, Langmuir (1995) 11, 2242
[30] C. C. Cheng, C. A. Chang, H. A. Yeh, Variable focus dielectric liquid droplet lens, Opt. Express (2006) 14, 4101
[31] S. K. Y. Tang, C. A. Stan, G. M. Whitesides, Dynamically reconfigurable liquid-core liquid-cladding lens in a microfluidic channel, Lab Chip (2008) 8, 395

[32] D.H. Doan, Y. Yin, N. Iwatani, K. Fushinobu, Laser processing by using fluidic laser beam shaper, Proc. National Heat Transfer Symposium 2012, Inpress

IntechOpen